Journal of Solid State Chemistry 182 (2009) 3171–3176

Contents lists available at ScienceDirect

Journal of Solid State Chemistry

journal homepage: www.elsevier.com/locate/jssc

Phase separation in the spin-state transition system of $La_{1-x}Ba_xCoO_3$

Wanju Luo *, Fangwei Wang

State Key Laboratory of Magnetism, Beijing National Laboratory for Condensed Matter Physics, Institute of Physics, Chinese Academy of Sciences, Beijing 100190, China

ARTICLE INFO

Article history:
Received 3 May 2009
Received in revised form
9 September 2009
Accepted 14 September 2009
Available online 19 September 2009

Keywords:
Spin-state transition
Phase separation
Phase diagram
Perovskite cobaltite

ABSTRACT

The magnetic and electric transport properties of $La_{1-x}Ba_xCoO_3$ ($0 < x \leq 0.50$) have been studied systematically. Two effects of substitution divalent ions on the spin-state transition of Co^{3+} have been differentiated for the substitution of Ba^{2+} for La^{3+} in $La_{1-x}Ba_xCoO_3$. The first is the transition from low-spin state to high-spin state due to lattice expansion, and the second is the transition from low-spin state to intermediate-spin state caused by the strong hybridization between ligand (oxygen) 2*p* and Co 3*d* orbital with introduction of holes in the oxygen 2*p* orbital. Based on the two different spin-state transition mechanisms and experimental results, a phase separation model has been developed and a very detailed magnetic and electric phase diagram of $La_{1-x}Ba_xCoO_3$ has been constructed.

1. Introduction

The perovskite cobaltite $LaCoO_3$ undergoes unique spin-state transitions on the changing of temperature, pressure and composition among transition metal oxide [1–3]. The magnetic susceptibility of $LaCoO_3$ exhibits two transitions at the temperature of about 100 and 500 K, which are always ascribed to spin-state transitions [1,4]. However, the nature of spin-state transitions has been a controversy for a long time. At the beginning, the first transition near 100 K was considered as low-spin (LS) ($S=0$, $t_{2g}^6 e_g^0$) to high-spin (HS) ($S=2$, $t_{2g}^4 e_g^2$) state transition of 50% of Co^{3+} while the second one near 500 K was ascribed to a transition from ordering to disordering of LS and HS [4,5]. This opinion was supported by the theoretical analysis of the traditional use of an ionic, ligand-field calculation [6]. But later LDA+U calculation revealed that strong hybridization between ligand (oxygen) 2*p* and Co 3*d* orbital stabilized the intermediate-spin (IS) ($S=1$, $t_{2g}^5 e_g^1$) state with introduction of holes in the oxygen 2*p* orbital. As results, the first transition near 100 K was explained as a transition from LS to IS state with orbital ordering whereas the second transition near 500 K was believed to be connected with a gradual disorder of occupied e_g orbitals within the IS state [7]. This explanation was so influential that most of the subsequent studies on cobaltites materials were interpreted in the transition of LS to IS state [8-11]. More recently both theory of a two-level model and X-ray absorption spectroscopy (XAS) and neutron spectroscopy experimental investigations confirm that the high-spin state interpretation is more appropriate than the intermediate-spin state [12–14].

Substitution of Sr^{2+} for La^{3+} in $La_{1-x}Sr_xCoO_3$ has been extensively studied for this system exhibiting spin-state transition and metal–insulator transition phenomena with different concentration *x* (and temperature changing), which is similar to the temperature varying induced spin-state transition in $LaCoO_3$, and other exciting behaviors such as spin glass and colossal magnetoresistance (CMR) [3,5,15–17]. Despite many achievements have been obtained and even some phase diagrams are constructed, the nature of spin-state transition in Sr^{2+}-doped $LaCoO_3$ is still controversial [10,14]. For the holes-doped transition metal oxides, phase separation is a key towards understanding of their physical properties. In $La_{1-x}Sr_xCoO_3$, several works confirm that this system phase separates into hole-rich magnetic and hole-poor nonmagnetic regions [18,19]. Ca^{2+} and Ba^{2+} with different ionic radii can introduce holes into Co–O bonds as Sr^{2+} does [20]. Unfortunately, however, much fewer studies reported the spin-state transition of Ca^{2+}- or Ba^{2+}-doped $LaCoO_3$. Especially, most studies for $La_{1-x}Ba_xCoO_3$ were focused on the transport properties [21–24]. In this paper the magnetization and resistivity of $La_{1-x}Ba_xCoO_3$ were studied systematically and a phase separation model was proposed to interpret the magnetic and electrical phenomena.

2. Experimental procedure and results

Polycrystalline samples of $La_{1-x}Ba_xCoO_3$ ($0.50 \geq x > 0$) were prepared by the standard solid-state reaction method using La_2O_3, $BaCO_3$ and Co_3O_4 powders. Structural characterization of the prepared samples was carried out using X-ray powder diffraction

* Corresponding author.
E-mail addresses: wanjuluo@msn.com (W. Luo), fwwang@aphy.iphy.ac.cn (F. Wang).

0022-4596/$ - see front matter © 2009 Elsevier Inc. All rights reserved.
doi:10.1016/j.jssc.2009.09.018

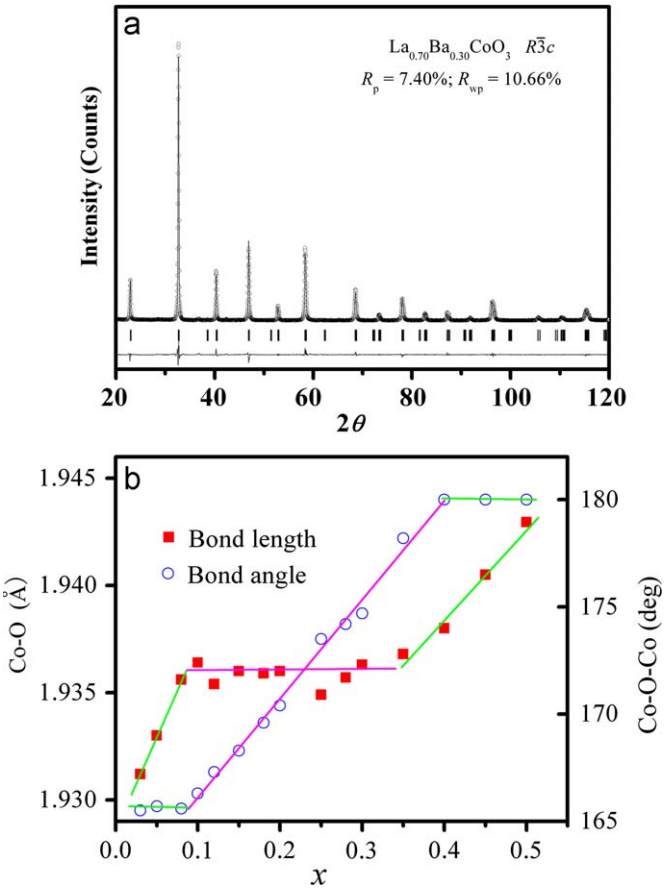

Fig. 1. (a) Representative Rietveld refined patterns corresponding to $La_{0.70}Ba_{0.30}CoO_3$ ($R\bar{3}c$) and (b) dependence of Co–O–Co bond angle and Co–O bond length of $La_{1-x}Ba_xCoO_3$ as a function of Ba concentration. The solid lines are guide to the eyes.

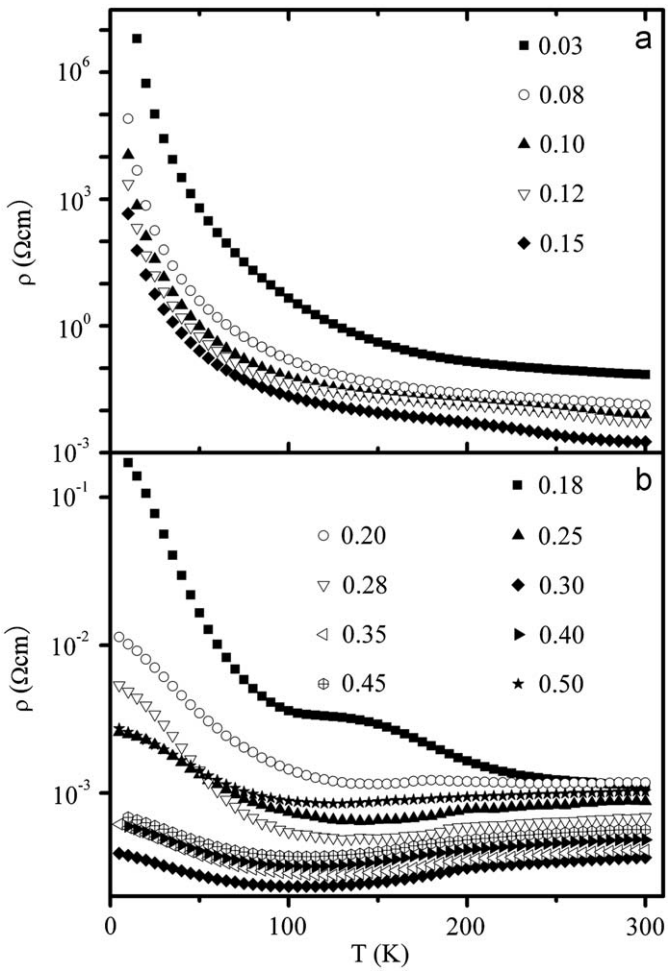

Fig. 2. Temperature dependences of resistivity in zero field for (a) the light-doped ($x < 0.18$) samples and (b) the highly doped ($0.18 \le x \le 0.50$) samples.

with Cu$K\alpha$ radiation on a Rigaku diffractometer. Resistivity was obtained via a standard dc four-probe method. Magnetization as a function of temperature was measured in warming after cooling in zero-field and in a field of 100 Oe from room temperature using SQUID MPMS-7.

XRD patterns confirmed that the samples were in high purity and Rietveld refinements were performed as represented by Fig. 1(a) and detailed in our previous work [25]. In brief, the Rietveld analysis revealed that the samples for $x \le 0.35$ had a rhombohedral phase with space group $R\bar{3}c$; whereas the samples for $x \ge 0.40$ had cubic structure with space group $Pm\bar{3}m$. One point should be clarified here is that a cubic structure was adopted for x=0.35 in our previous work based on the little better refinement indices. Subsequent neutron powder diffraction justified that a rhombohedral phase would be much better than a cubic one for x=0.35 [25]. The evolution of the CoO_6 octahedron was redrawn as shown in Fig. 1(b). The evolution of the CoO_6 can be divided into three regions as indicated by the solid line in the figure. For $x < 0.1$, the Co–O bond length of the CoO_6 octahedron expands with increasing Ba content, and then levels off at $0.1 \le x < 0.4$, at the end of which the Co–O–Co bond angle reaches 180°. The expansion of the Co–O bond length resumes with further increase in Ba dopant when $0.4 \le x \le 0.5$.

The temperature dependences of the zero-field resistivity (ρ) with different Ba doping are displayed in Fig. 2. As the effect of doping divalent Sr, doping Ba results in hole doping and the eventual onset of metallic behavior. The samples for $0 < x < 0.18$ display insulator behavior in the whole temperature as shown in Fig. 2(a), whereas other samples for $x > 0.18$ behave as metal at high temperature and metal–insulator transition (MIT) is generated below a critical point at low temperature as shown in Fig. 2(b). This MIT in the higher-doped samples may be caused due to the grain boundary scattering in the poorly sintered samples and it disappears in single crystals [26]. Considering the mechanism of conductivity in the divalent ion-doped $LaCoO_3$, the minimum electrical resistivity should be reached at x=0.5 [15–17]. However, just like the previous reported works [21–23], the minimum in the barium compounds was obtained at x=0.30 in this work. This deviation may be caused by the oxygen deficient in the high-doped samples.

Fig. 3 shows the representatives of the temperature dependences of the dc magnetization. These data were taken on heating under an external field of 100 Oe after cooling in zero magnetic field (ZFC) or in a field of 100 Oe (FC). Just like the system of $La_{1-x}Sr_xCoO_3$, $La_{1-x}Ba_xCoO_3$ can be divided into two groups due to the different magnitudes of magnetization: $0 < x < 0.18$ and $0.18 \le x \le 0.50$. In Fig. 3 the upper panels of (a), (b) and (c) are representatives of all compositions in the range of $0 < x < 0.18$, while the lower panels of (d), (e) and (f) are specimens of the samples in the range $0.18 \le x \le 0.50$. With decreasing temperature, in the range of $0 < x < 0.18$ the ZFC curves increase and show very sharp peaks at a temperature (the peak temperature, T_p) far below T_C, while the FC magnetization monotonically increases more prominently below the irreversibility temperature T_{irr}, at which the bifurcation between ZFC and FC occurs. This magnetic behavior has been interpreted in terms

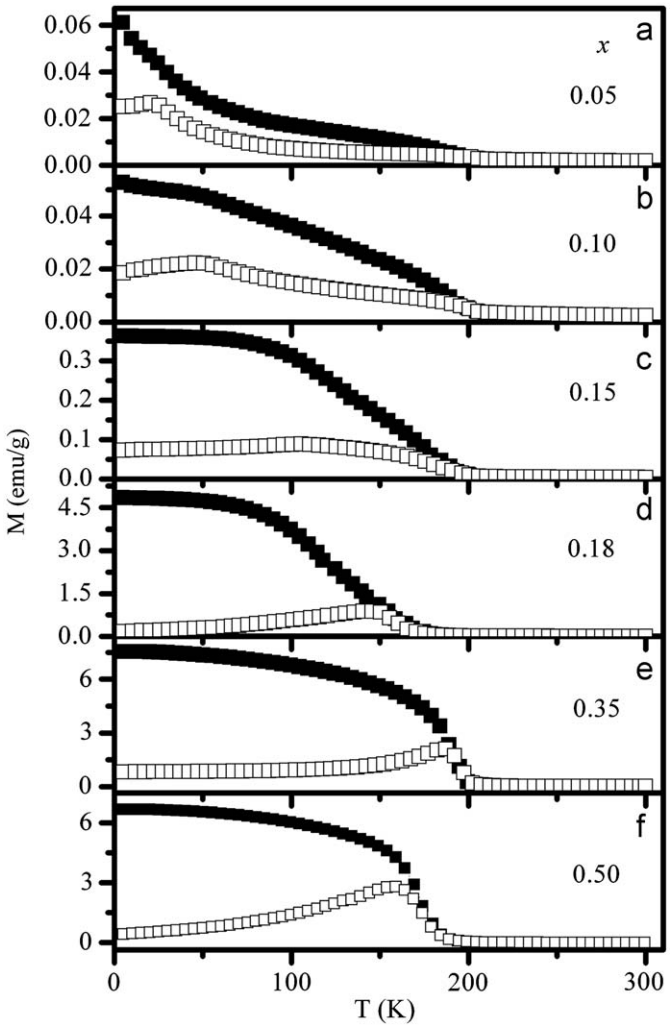

Fig. 3. Temperature dependences of the dc magnetization in a field of 100 Oe for x=0.05 (a), x=0.10 (b), x=0.15 (c), x=0.18 (d), x=0.35 (e) and x=0.50 (f). ZFC curves are shown as open symbols, whereas FC curves are shown as solid symbols.

of spin glass by several authors in previous work on $La_{1-x}Sr_xCoO_3$ and $La_{1-x}Ba_xCoO_3$ in the corresponding range [19,27,28].

When x increases to a critical value of 0.18, the FC curves increase prominently near T_C with decreasing temperature and level off at low temperature, showing a "Brillouin-like" temperature dependence of the magnetization. In contrast, the ZFC magnetization is rather small and peaks at a little below T_C. These magnetic phenomena were interpreted as cluster glass in previous studies [19,27,28]. On the other hand, some neutron data suggest real long-range ordered ferromagnetism in the high-doped $LaCoO_3$ and the splitting between ZFC and FC curves are explained as the symptom of the strong anisotropy of ferromagnets [29–31]. Considering the dynamic magnetic properties of $La_{1-x}Ba_xCoO_3$ and $La_{1-x}Sr_xCoO_3$, it seems that the interpretation of cluster glass is more appropriate than the ferromagnetism one [32,33].

To clarify the critical problem of spin states in $La_{1-x}Ba_xCoO_3$, we extracted the effective numbers of Bohr magnetons from the Curie–Weiss law in the paramagnetic phase at $T > T_C$. The susceptibility of the paramagnetic phase follows the Curie–Weiss law,

$$\chi = \frac{C}{T-\theta}, \tag{1}$$

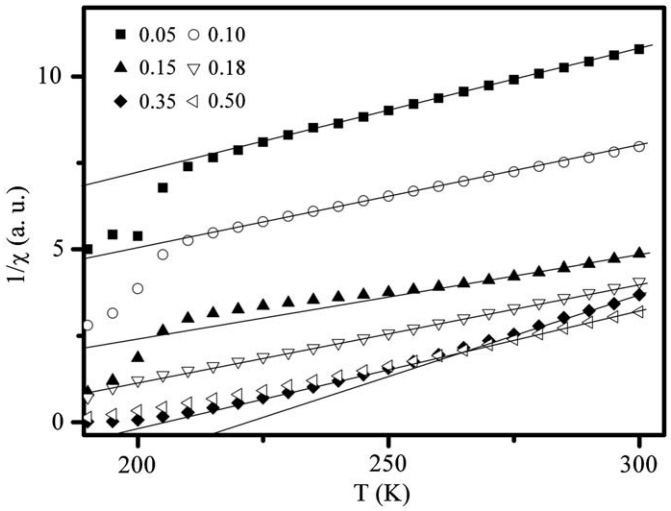

Fig. 4. Representative temperature dependences of the inverse magnetic susceptibility.

where

$$C \propto \frac{\mu_{\text{eff}}^2}{3k_B} \text{ and } \mu_{\text{eff}} = g[J(J+1)]^{1/2}\mu_B. \tag{2}$$

Here, χ is the susceptibility, C is the Curie constant, $\theta \approx T_C$, k_B is the Boltzmann constant and μ_{eff} is the effective numbers of Bohr magnetons (μ_B). g is the Landé g-factor, and J is the total spin quantum number. For transition metals J equals to S due to the orbital quenching. As shown in Fig. 4 derived from Fig. 3, for all x values Eq. (1) describes the data very well above T_C. The spin of Co^{3+} and Co^{4+} in configuration of low-spin state, intermediate-spin state, and high-spin state are 0, 1 and 2, and 1/2, 3/2 and 5/2, respectively. Hereafter, for the convenience of description, the ions of Co^{3+} and Co^{4+}, in the configurations of low-spin, intermediate-spin and high-spin states, will be denoted as Co(III)/Co(IV), Co(iii)/Co(iv) and Co^{3+}/Co^{4+}, respectively.

3. Spin-state analysis and discussion

Fig. 5(a) displays the effective Bohr magneton numbers derived from the temperature dependence of magnetization by Curie–Weiss law. To get insight on the spin state of the Co ions, the formula (2) with Landé g-factor g=2 and quantum number J=S, assuming certain spin configurations, is adopted.

On the hypothesis of simple spin configurations as usually used in previous works [8,28], the effective numbers are obtained by

$$\mu_{\text{eff}}^2 = (1-x)\mu_{\text{Co}^{3+}}^2 + x\mu_{\text{Co}^{4+}}^2. \tag{3}$$

Different combinations of spin-state configurations are assumed to reproduce the effective numbers and some representative results are shown in Fig. 5(a). Obviously, as shown in the figure, simple spin-state configurations are not adequate to reproduce the experimental data. In order to get better fitting to the experimental data, many different configurations are trailed. As a result, a phase separation model is developed and will be described below.

Substitution of Ba^{2+} for La^{3+} in $La_{1-x}Ba_xCoO_3$ has two effects: hole introducing and lattice expansion [34–37]. With substitution of divalent Ba^{2+} ions for La, tetravalent Co with IS state Co(iv) is induced and the surroundings of LS state Co(III) are converted to IS Co(iii) due to strong hybridization between ligand (oxygen) 2p

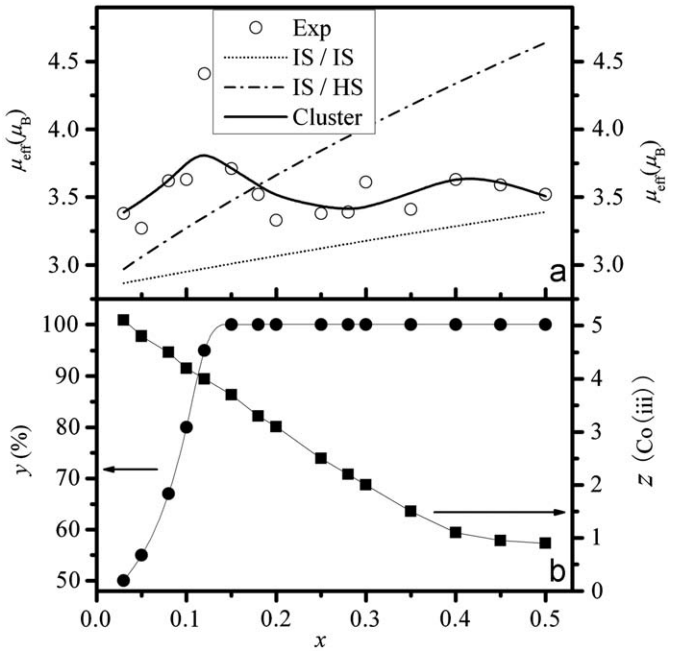

Fig. 5. x dependence of (a) the effective Bohr magneton numbers extracted from the Curie–Weiss law above T_C (open circles) and different calculations (lines), (b) the percentage y of the high-spin state Co^{3+} in the nonmagnetic matrix and the average number z of Co(iii) in the unit of Co(iv)zCo(iii). In (a), the dotted line represents the calculated results assuming all Co ions in IS states. The broken line assumes IS Co(iii) and HS Co^{4+}. The solid curve is the results calculated from the phase separation hypothesis as described in this paper.

and Co 3d orbital with introduction of holes in the oxygen 2p orbital [7]. Naturally, a cluster unit of Co(iv)6Co(iii) is formed. The cluster units are connected to each other by a link of Co(iii) with increasing Ba^{2+} concentration. As a result the average number of Co(iii) attached to Co(iv) is reduced and the form of the cluster unit would be replaced by an average unit of Co(iv)zCo(iii). Thus, a magnetic cluster, nCo(iv)zCo(iii), is constructed by n average cluster units of Co(iv)zCo(iii). For light-doped compounds, there is non-interaction between the clusters. Thus these clusters belong to superparamagnetic cluster, which were proved in our previous work [38]. With increase in concentration x, the size of clusters increases and the magnetization becomes stronger and stronger, while the distance between clusters decreases. Once the concentration x reaches the magnetic critical concentration x_c, the interaction between neighboring clusters will be brought out, and the samples behave as cluster glass [39].

At low temperature, the parent compound $LaCoO_3$ is located at the low-spin nonmagnetic ground state [5,7]. With temperature increased to 100 K, 50% LS Co(III) transfers to HS Co^{3+} due to thermal expansion. Thus, orbital ordered 50% LS Co(III) and 50% HS Co^{3+} matrix is constructed in the temperature range from about 100 to 300 K. With Ba^{2+} substitution for La^{3+} at low temperature, two kinds of regions are formed: cluster region of nCo(iv)zCo(iii) and hole-poor region. In the hole-poor region, part of LS Co(III) ions transfer to HS Co^{3+} state due to the doping effect of lattice expansion and the ratio of HS Co^{3+} increases with increase in Ba^{2+} concentration. These Co(III) and Co^{3+} were divided into two phases of orbital ordered Co(III)-Co^{3+} matrix and antiferromagnetic (AF) Co^{3+}–Co^{3+} matrix, and their ratio varies according to different concentrations x [5,8,40].

Based on the above description of phase separation, the chemical formula of $La_{1-x}Ba_xCoO_3$ could be written as follows:

$$La_{1-x}Ba_x[\mathrm{Co(iv)Co(iii)}_z]_x\{[\mathrm{Co(III)Co}^{3+}]_{1-y}\mathrm{Co}^{3+}_{2y-1}\}_{1-x(1+z)}\mathrm{O}_3\ (z\geq 1),$$

and

$$\mathrm{La}_{1-x}\mathrm{Ba}_x\{[\mathrm{Co(iv)Co(iii)}]_z\mathrm{Co(iv)}_{1-z}\}_x\mathrm{Co}^{3+}_{1-x(1+z)}\mathrm{O}_3,\ (z<1).$$

In the chemical formula, y represents the percentage of Co^{3+} in the ordered matrix Co(III)–Co^{3+} and AF Co^{3+}–Co^{3+}, and that z indicates the average number of Co(iii) attaching to Co(iv). The physical properties of z and y are evident: z representing the ability of introducing holes for Ba^{2+} ions and it ranges from 0 to 6, and y indicating the lattice expansion effect due to a large ionic radius of Ba^{2+} compared with that of La^{3+} ion [37].

Based on the above hypothetical phase separation description, once the parameters of y and z are given, the effective Bohr magneton numbers can be calculated as follow:

$$\mu_{\mathrm{eff}}^2 = x\mu_{\mathrm{Co(iv)}}^2 + zx\mu_{\mathrm{Co(iii)}}^2 + y[1-x(1+z)]\mu_{\mathrm{Co}^{3+}}^2. \quad (4)$$

The calculated results of phase separation hypothesis, as illustrated by the solid curve in Fig. 5(a), are obtained by adopting the values of y and z as shown in Fig. 5(b). The values of y and z are determined as follow. First, y and z should be kept reasonable for their physical properties: at the end compound $LaCoO_3$ y equals to 50%, and it increases with increase in Ba^{2+} concentration, while it should not exceed 100% for the ordered matrix changing from Co(III)–Co^{3+} to Co^{3+}–Co^{3+}. The z value should range from 6 to 0 for the average cluster Co(iv)zCo(iii) starts from Co(iv)6Co(iii) to Co(iv)Co(iv). Second, the results should be calculated by minimizing the mean square error.

Obviously the phase separation results, assuming the spin-state combination as described above, are far better than that of others. The phase separation results confirm that LS Co(III) is converted to HS Co^{3+} completely for the value of y reaches 100% between Ba concentrations x=0.12 and x=0.15, and a fourth phase of Co(iv)–Co(iv) appears at $x>0.40$ for $z<1$. Both of the critical y and z are corroborated by the three-phase expansion of CoO_6 octahedron with doping as shown in Fig. 1(b): $x<0.1$, $0.1\leq x<0.4$, and $0.4\leq x\leq 0.5$. There are little differences between the critical values deduced from the phase separation model and the structural transition points of CoO_6. The reason could be that the values of phase separation model reflect the evolution of partial Co ions while the later denotes the evolution of the average value of all Co ions. On the other hand, they may be also caused by the magnetic results derived from the oxygen deficiency in the samples.

Combining the above analysis and the experimental results of the magnetic and electrical measurements, a detailed phase diagram of $La_{1-x}Ba_xCoO_3$ has been constructed as shown in Fig. 6. The different meaning of all kinds' abbreviations and the boundaries between different regions in the phase diagram are described in the explication of the figure. Addition to the explication in the figure, several points should be marked. First, there is paramagnetic insulator phase of Co(III)Co^{3+} in the region of $0<x<0.15$. Second, the boundary of the AF cluster insulator plus superparamagnetic cluster metal is drawn roughly for it is hard to differentiate the temperature of phase transition due to the disturbance of the superparamagnetic cluster freezing effect. Last, the evolution of the fourth phase Co(iv)–Co(iv) has not been determined in that there are not enough data about it.

In the frame of phase separation model, the measurable physical properties of a sample should be considered as collective effect of all contributions from different phases plus the coupling effect at the boundaries. At ground state T=0 K, the configurations of Co(III) and Co^{3+} are $t_{2g}^6e_g^0$ and $t_{2g}^4e_g^2$, respectively [5]. LS Co(III) attaches to HS Co^{3+} via a smaller covalent bond and the matrix is paramagnetic insulating system due to orbital ordering of Co(III)–Co^{3+} below room temperature [38]. The interaction in the matrix of Co^{3+}–Co^{3+} is AF superexchange. At low temperature for small x, this matrix is short-range-ordered AF interacting cluster insulator

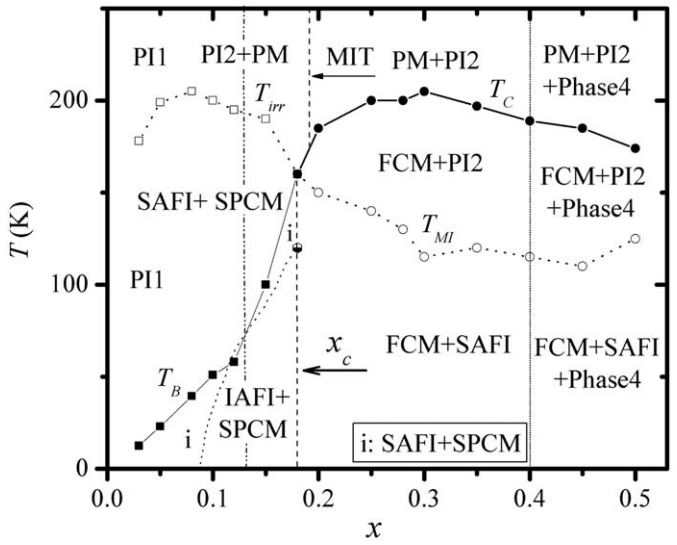

Fig. 6. The magnetic and electrical phase diagram of $La_{1-x}Ba_xCoO_3$. PI1, PI2, PM, SPCM, FCM, IAFI and SAFI denote paramagnetic insulator of the Co(III)–Co^{3+} matrix, paramagnetic insulator of Co^{3+}–Co^{3+} matrix, paramagnetic metal of Co(iv)*z*Co(iii), superparamagnetic cluster metal of *n*Co(iv)*z*Co(iii), ferromagnetic cluster glass metal of *n*Co(iv)*z*Co(iii), intermediate-range-ordered AF interacting insulator of Co^{3+}–Co^{3+}, short-range-ordered AF interacting insulator of Co^{3+}–Co^{3+}, respectively. The fourth phase is AF interacting Co(iv)–Co(iv). T_{irr}, T_C, T_B and T_{MI} represent the temperature of bifurcation between the dc magnetization of ZFC and FC, the ferromagnetic Curie temperature, the freezing temperature of the superparamagnetic cluster, and the metal–insulator transition temperature, respectively. x_c indicates the critical concentration. The dash–dot–dot line near $x=0.12$ implies the disappearance of orbital ordered Co(III)Co^{3+}. The short-dot line at $x=0.4$ suggests the fourth phase is set.

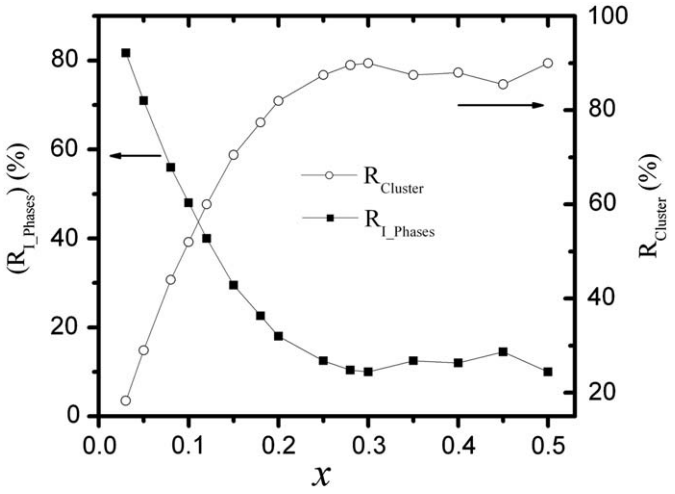

Fig. 7. The *x* dependence for the sum concentration of the insulating phases R_{I_phases} and for the sum concentration of Co(iv) and C(iii) in the cluster of *n*Co(iv)*z*Co(iii) $R_{cluster}$.

due to the isolation of nonmagnetic Co(III)–Co^{3+} matrix. When the concentration reaches $x=0.10$, the short-range-ordered AF interacting matrix becomes intermediate-range-ordered AF interacting cluster insulator with Co^{3+} increasing. The AF interacting matrix transfers to paramagnetic insulator with temperature increasing. The phase of *n*Co(iv)*z*Co(iii) is superparamagnetic cluster (which grows in size and number with increase in *x*) dominated by ferromagnetic double-exchange interaction between Co(iv) and Co(iii) at low temperature for $x<0.18$. Once the growing size of the cluster exceeds a certain value beyond the critical value $x_c=0.18$, the neighboring cluster interaction is brought out due to the stronger and stronger magnetization and shorter and shorter distance. With *x* increasing, a fourth phase of Co(iv)–Co(iv) appeared at $x>0.40$ for $z<1$. Another point should be strengthened is that the competition between the ferromagnetic cluster glass and the surrounding AF interacting matrix of Co^{3+}–Co^{3+} makes the AF matrix to be short-range-ordered AF cluster rather than intermediate-range-ordered AF cluster beyond x_c. In the whole range of *x*, the short-range-ordered AF insulator converts to paramagnetic insulator at Néel temperature T_N, and the clusters of *n*Co(iv)*z*Co(iii) transfer to paramagnetic metal at T_C with increase in temperature.

The quantitative change for different phases with increase in *x* could be calculated based on the values of *y* and *z*, and their two groups are shown in Fig. 7. R_{I_phases} refers to the sum concentration of insulated phases of PM Co(III)–Co^{3+}, AF Co^{3+}–Co^{3+} and AF Co(iv)–Co(iv), while $R_{cluster}$ represents the concentration of FM *n*Co(iv)*z*Co(iii). According to the evolutions of properties and quantity (indicated in Fig. 7) for different phases, it is naturally educed that the temperatures (T_{irr}) of bifurcation between the dc magnetization of ZFC and FC, and Curie temperature T_C indicate a transition of cluster from ferromagnetic to paramagnetic phase. The metal–insulator transition temperature (T_{MI}) reflects the transition from AF insulator (Co^{3+}–Co^{3+}) to paramagnetic insulator. On the other hand, the metal–insulator transition at low *T* for the higher-doped samples could also be obtained in the poorly sintered samples due to grain boundary scattering. The peak temperature T_p in ZFC curves might be the blocking temperature of superparamagnetic cluster. That is to say, the nature of freezing effect might be the transition temperature superparamagnetic state to blocking state in $La_{1-x}Ba_xCoO_3$ for $x<0.18$. The spin-glass like phenomenon for the samples of $x<0.18$ could be originated from the freezing effect of the local anisotropy in the superparamagnetic cluster. The abnormal behavior beyond $x=0.40$ should be answered by the fourth phase Co(iv)–Co(iv). The interaction between Co(iv)–Co(iv) is AF superexchange. Therefore the short-range-ordered AF effect has been strengthened and the ferromagnetic cluster properties have been restrained.

4. Summary and conclusions

A phase separation model has been proposed to understand the spin-state transition properties in $La_{1-x}Ba_xCoO_3$. Combining the experimental data and the phase separation analysis, a detailed phase diagram of $La_{1-x}Ba_xCoO_3$ has been constructed. The hypothesis of phase separation favors that the spin-state transition in $LaCoO_3$ near 100 K is LS to HS transition. Based on the properties and quantitative analysis of different phases, new mechanisms are proposed to interpret the nature of the peak temperature T_p and the irreversible temperature T_{irr}. The bifurcation between ZFC and FC magnetization curves in cobaltites is the Curie temperature of superparamagnetic clusters. The peak temperature might be the blocking temperature for low concentration *x*, and the spin-glass like behavior is ascribed to the freezing effect of the local anisotropy field in superparamagnetic clusters.

Acknowledgments

This work was supported by the Natural Science Foundation of China (Contract no 10375088).

References

[1] G. Vanko, J.P. Rueff, A. Mattila, Z. Németh, A. Shukla, Phys. Rev. B 73 (2006) 024424.
[2] R. Lengsdorf, M. Ait-Tahar, S.S. Saxena, M. Ellerby, D.I. Khomskii, H. Micklitz T. Lorenz, M.M. Abd-Elmeguid1, Phys. Rev. B 69 (2004) 140403(R).
[3] M. Itoh, I. Natori, S. Kubota, K. Motoya, J. Phys. Soc. Jpn. 63 (1994) 1486.
[4] J.B. Goodenough, J. Phys. Chem. Solids 6 (1958) 287.
[5] M.A. Senaris, J.B. Goodenough, J. Solid State Chem. 118 (1995) 323.
[6] Y. Tanabe, S. Sugano, J. Phys. Soc. Jpn. 9 (1954) 766.
[7] M.A. Korotin, S.Y. Ezhov, I.V. Solovyev, V.I. Anisimov, D.I. Khomskii G.A. Sawatzky, Phys. Rev. B 54 (1996) 5309.
[8] J. Wu, C. Leighton, Phys. Rev. B 67 (2003) 174408.
[9] C. Zobel, M. Kriener, D. Bruns, J. Baier, M. Gruninger, T. Lorenz, P. Reutler A. Revcolevschi, Phys. Rev. B 66 (2002) 020402(R).
[10] T. Vogt, J.A. Hriljac, N.C. Hyatt, P. Woodward, Phys. Rev. B 67 (2003) 140401(R).
[11] R.F. Klie, J.C. Zheng, Y. Zhu, M. Valera, J. Wu, C. Leighton, Phys. Rev. Lett. 99 (2007) 047203.
[12] S.W. Biernachi, Phys. Rev. B 74 (2006) 184420.
[13] M.W. Haverkort, Z. Hu, J.C. Cezar, T. Burnus, H. Hartmann, M. Reuther, C. Zobel, T. Lorenz, A. Tanaka, N.B. Brookes, H.H. Hsieh, H.J. Lin, C.T. Chen, L.H. Tjeng, Phys. Rev. Lett. 97 (2006) 176405.
[14] A. Podlesnyak, S. Streule, J. Mesot, M. Medarde, E. Pomjakushina, K. Conder A. Tanaka, M.W. Haverkort, D.I. Khomskii, Phys. Rev. Lett. 97 (2006) 247208.
[15] R. Mahendiran, A.K. Raychaudhuri, Phys. Rev. B 54 (1996) 16044.
[16] D. Phelan, D. Louca, S. Rosenkranz, S.H. Lee, Y. Qiu, P.J. Chupas, R. Osborn H. Zheng, J.F. Mitchell, J.R.D. Copley, J.L. Sarrao, Y. Moritomo, Phys. Rev. Lett. 96 (2006) 027201.
[17] J. Wu, J.W. Lynn, C.J. Glinka, J. Burley, H. Zheng, J.F. Mitchell, C. Leighton, Phys. Rev. Lett. 94 (2005) 037201.
[18] D. Phelan, D. Louca, K. Kamazawa, S.H. Lee, S.N. Ancona, S. Rosenkranz Y. Motome, M.F. Hundley, J.F. Mitchell, Y. Moritomo, Phys. Rev. Lett. 97 (2006) 235501.
[19] R. Caciuffo, R. Caciuffo, D. Rinaldi, G. Barucca, J. Mira, J. Rivas, M.A. Senarıs-Rodrıguez, P.G. Radaelli, D. Fiorani, J.B. Goodenough, Phys. Rev. B 59 (1999) 1068.
[20] M. Kriener, C. Zobel, A. Reichl, J. Baier, M. Cwik, K. Berggold, H. Kierspel O. Zabara, A. Freimuth, T. Lorenz, Phys. Rev. B 69 (2004) 094417.
[21] S.B. Patil, H.V. Keer, D.K. Chakrabarty, Phys. Status Solidi (a) 52 (1979) 681.
[22] A. Barman, M. Ghosh, S.K. De, S. Chatterjee, Phys. Lett. A 234 (1997) 384.
[23] P. Mandal, P. Choudhury, S.K. Biswas, B. Ghosh, Phys. Rev. B 70 (2004) 104407.
[24] M.S. Khalil, Mater. Sci. Eng. A 352 (2003) 64.
[25] W. Luo, F. Wang, Powder Diffr. 21 (2006) 304.
[26] S. Yamaguchi, H. Taniguchi, H. Takagi, T. Arima, Y. Tokura, J. Phys. Soc. Jpn. 64 (1995) 1885.
[27] N. Menyuk, P.M. Raccah, K. Dwight, Phys. Rev. 166 (1968) 510.
[28] V.G. Bhide, D.S. Rajoria, C.N.R. Rao, G.R. Rao, V.G. Jadhao, Phys. Rev. B 12 (1975) 2832.
[29] V.G. Sathe, A.V. Pimpale, V. Siruguri, S.K. Paranjpe, J. Phys. Condens. Matter 8 (1996) 3889.
[30] R. Ganguly, I.K. Gopalakrishnan, J.V. Yakhmi, Physica B 271 (1999) 116.
[31] A.P. Sazonov, I.O. Troyanchuk, H. Gamari-Seale, V.V. Sikolenko, K.L. Stefanopoulos, G.K. Nicolaides, Y.K. Atanassova, J. Phys. Condens. Matter 21 (2009) 156004.
[32] S. Mukherjee, R. Ranganathan, P.S. Anilkumar, P.A. Joy, Phys. Rev. B 54 (1996) 9267.
[33] D.N.H. Nam, K. Jonason, P. Nordblad, N.V. Khiem, N.X. Phuc, Phys. Rev. B 59 (1999) 4189.
[34] W. Luo, F. Shi, F. Wang, J. Magn. Magn. Mater. 305 (2006) 509.
[35] K. Muta, Y. Kobarashi, K. Asai, J. Phys. Soc. Jpn. 71 (2002) 2784.
[36] P.G. Radaelli, S.W. Cheong, Phys. Rev. B 66 (2002) 094408.
[37] R.D. Shannon, Acta Cryst. A 32 (1976) 751.
[38] W. Luo, F. Wang, J. Magn. Magn. Mater. 321 (2009) 1280.
[39] W. Luo, F. Wang, Appl. Phys. Lett. 90 (2007) 162515.
[40] G. Maris, Y. Ren, V. Volotchaev, C. Zobel, T. Lorenz, T.T.M. Palstral, Phys. Rev. B 67 (2003) 224423.